AIMS Mathematics, 8(11): 27009–27032.
DOI: 10.3934/math.20231382
Received: 23 June 2023
Revised: 17 August 2023
Accepted: 30 August 2023
Published: 22 September 2023

http://www.aimspress.com/journal/Math

Research article

Analyzing a SEIR-Type mathematical model of SARS-COVID-19 using piecewise fractional order operators

Nadiyah Hussain Alharthi and Mdi Begum Jeelani*

Department of mathematics and statistics, College of Science, Imam Mohammad Ibn Saud Islamic University (IMSIU), Riyadh, Saudi Arabia

* **Correspondence:** Email: mbshaikh@imamu.edu.sa, write2mohammadi@gmail.com.

Abstract: Recently, the area devoted to mathematical epidemiology has attracted much attention. Mathematical formulations have served as models for various infectious diseases. In this regard, mathematical models have also been used to study COVID-19, a threatening disease in present time. This research work is devoted to consider a SEIR (susceptible-exposed-infectious-removed) type mathematical model for investigating COVID-19 alongside a new scenario of fractional calculus. We consider piece-wise fractional order derivatives to investigate the proposed model for qualitative and computational analysis. The results related to the qualitative analysis are studied via using the tools of fixed point approach. In addition, the computational analysis is performed due to a significance of simulation to understand the transmission dynamics of COVID-19 infection in the community. In addition, a numerical scheme based on Newton's polynomials is established to simulate the approximate solutions of the proposed model by using various fractional orders. Additionally, some real data results are also shown in comparison to the numerical results.

Keywords: dynamical system; piecewise derivative; Newton polynomials; fractional order iterative method
Mathematics Subject Classification: 34A08, 47H08, 93A30

1. Introduction

It is now recognized that a recent outbreak of acute atypical respiratory infections with an origin in Wuhan, China, was caused by the novel coronavirus known as the severe acute respiratory syndrome (SARS) coronavirus-2. The coronavirus disease 19 (COVID-19), which is the illness brought on by this virus, has spread alarmingly quickly over the world and was classified as a pandemic by the World Health Organization (WHO) on March 11, 2020 (see [1–3]). More than six million deaths attributed to COVID-19 have been documented globally. Approximately 600 to 700 people in the same line

have an infection. The state of the economy, people's health, and their way of life have all been severely disrupted. Researchers and scientists are working around the clock to find the best treatment for COVID-19 (see [4]). Every state in the globe has already seized it. Here, we remark that people can spread the virus to one another by exchanging respiratory droplets and aerosols. After entering the body, the virus connects to the host receptors and enters the host cells via either membrane fusion or endocytosis. The four structural proteins of the coronaviruses' are the spike, membrane, envelope, and nucleocapsid proteins are the coronaviruses' four structural proteins (see details [5]). Currently, COVID-19 causes 300 to 500 fatalities every day in the United States, which is an annual mortality load greater than that brought on by an unfavorable influenza season. In the same way, in other localities of the word, the virus appears in different shapes and is the cause for disease in society. To date, the suggested or required preventative measures have been moulded by a number of epidemiologic and clinical assessments that have been used to monitor the effects of COVID-19. The estimated rates of COVID-19 cases, hospitalizations, and fatalities have typically been included in these measurements. Monitoring of circulating SARS-CoV-2 variations and their susceptibility to existing vaccines and therapies has also been performed (see details [6]).

Because of advances in technology, epidemiology has advanced to the point where different infectious diseases are examined for treatment, control, curing, and so on [7]. Here, it should be noted that mathematical biology also plays a significant part in the investigation of many diseases. As a result, significant progress has been made in the mathematical modelling of infectious diseases over the previous many decades [8,9]. In terms of research, mathematical modelling has grown in popularity during the previous three decades. Mathematical models aid in the development of secure public health methods for the successful control of various diseases [10]. These mathematical models are useful for studying spatiotemporal patterns and the dynamic behaviour of infections. With the importance of mathematical models, academics have researched COVID-19 from many perspectives over the last three years [5]. Researchers in this field are employing a variety of approaches to develop successful techniques for controlling this condition (some recent studies are included in [11, 12]). Recently, a mathematical model was employed to investigate the impacts of immunization in nursing homes, for example, see [13]. Researchers investigated mathematical modeling and effective intervention options for the COVID-19 outbreak [14]. Recently, some writers investigated COVID-19 mathematical models using stochastic differential equations and environmental white noise [15–18].

As we know, the field of epidemiology has been thoroughly researched using the idea of classical derivatives. Because classical differential operators are local, they cannot adequately explain a variety of inherited, short and long memory processes. As a result, fractional calculus has received increased attention in recent decades in order to more thoroughly understand the aforementioned process. Its dynamic characteristics have demonstrated a wide range of applications in real-world situations such as biological and physical phenomena thereby increasing its popularity [19]. Just like regular calculus, fractional calculus has a long history [20]. Several authors have explored the said topic from various perspectives; we refer to a few as [21–23]. The aforementioned calculus has numerous applications in science and technology (see [24, 25]).

Although it has a history that is as old as classical calculus, fractional derivatives are significantly less well-known than they ought to be. What does the term "fractional derivative" mean physically? This issue is still unresolved. We find that a memory process typically has two stages after modelling various memory events. One has permanent retention and is short, whereas the other is controlled

by a straightforward fractional derivative model (see [26–29]). Using the numerical least squares method, we demonstrate how the fractional model fully fits the test data of memory phenomena in other disciplines, including biology, psychology and mechanics. This approach leads us to the conclusion that the fractional order has an index of memory as its physical meaning (see [30–33]).

The majority of real-world problems have some degree of unpredictability that traditional mathematical models cannot capture. In recent decades, the concept of stochastic mathematical differential equations has been proposed and widely employed, with notable results. However, rather than following randomness, other problems follow non-locality trends, such as long-range dependence, fractal processes, power law processes, and crossover behaviors, implying that physical events exhibit a wide range of behaviors. To address these issues, a class of fractional derivatives was suggested, which includes fractional differential operators with singular type kernels, fractal fractional operators, and differential operators with regard to other functions. However, these operators are still poor at characterizing crossover behavior. The idea of a short memory fractional order derivative was developed for the first time to characterize the aforementioned behavior. Although fractional derivatives have an extended memory capability, the piecewise notion has been shown to be more powerful than described (see details in [34]). To examine the crossover properties, we introduce several notions such as the fractal-fractional derivative, the fractional order derivative with singular and non-singular kernels, and some other forms of derivative operators. For example, [35] refers to some valuable work on nonlocal operators and their applications; [36] refers to a mathematical model under the Caputo-Fabrizio operator; [37] refers to the fractional dynamics of cellulose degradation; [38] refers to local and nonlocal operators with applications; and [39] refers to the existence and uniqueness with applications to epidemiology. Although randomness considerations in the framework of the stochastic equation produce more realistic results, the crossover dynamical behavior has not been studied [40]. Many real-world process models, such as heat flow, fluid flow, and many complex advection problems, exhibit this behavior (see [41]). The exponential and Mittag-Leffler mappings cannot find the timing of crossovers in fractional calculus because many real-world issues exhibit crossover behavior that is not adequately characterized by the standard fractional order derivative. Due to phenomena such as earthquakes, pendulum motion, the volatility of the economy in less developed countries at the present moment are experiencing rapid changes in their state of rest or uniform motion. Using piecewise equations with fractional order derivatives, this crossover behavior can be clearly demonstrated. Recently, in this regard, some essential aspects have been identified by analyzing various models in [42]. The authors developed classical and global piecewise derivatives, as well as various applications. Recently, various infectious disease models have been examined employing non-singular and power-law type operators, as shown in [43–48].

Keeping the above importance, we intend to focus on these fundamental problems in this study, utilizing a model specifically adapted to reflect the hallmark of the COVID 19 dynamics, as well as the constraints in our reaction to it. First, we replicate the epidemic dynamics inside one community with a specific social pattern, using a conventional SEIR design that allows for long incubation. Here, we formulate our model under piecewise derivative as follows:

$$\begin{cases} {}^{PCC}_{0}\mathbb{D}^{\mathrm{r}}_{t}(S)(t) &= \mathbf{a} - \frac{\rho_1 SI}{1+\gamma I} - (\delta + p)S \\ {}^{PCC}_{0}\mathbb{D}^{\mathrm{r}}_{t}(E)(t) &= pS - \delta E - \rho_2 \alpha EI \\ {}^{PCC}_{0}\mathbb{D}^{\mathrm{r}}_{t}(I)(t) &= \frac{\rho_1 SI}{1+\gamma I} + \rho_2 \alpha EI - (\delta + \mu_0 + w - \mathbf{b})I \\ {}^{PCC}_{0}\mathbb{D}^{\mathrm{r}}_{t}(R)(t) &= wI - \delta R, \end{cases} \tag{1.1}$$

where ${}_0^{PCC}\mathbb{D}_t^{\mathrm{r}}$ stands for piecewise Caputo derivative which can be described for any function say y as

$$ {}_0^{PCC}\mathbb{D}_t^{\mathrm{r}}(y(t)) = \begin{cases} {}_0^{C}\mathbb{D}_t(y(t)) = \dfrac{dy}{dt}, \quad 0 < t \leq t_1, \\ {}_0^{C}\mathbb{D}_t^{\mathrm{r}}(y(t)) = \dfrac{1}{\Gamma(1-\mathrm{r})} \displaystyle\int_{t_1}^{t_2} (t-\eta)^{-\mathrm{r}} y'(\eta) d\eta, \quad t_1 < t \leq t_2, \end{cases} \tag{1.2} $$

where ${}_0\mathbb{D}_t^{\mathrm{r}}$ represents the usual Caputo fractional order derivative. The flow chart of our model is given in Figure 1, while the parameters and nomenclatures are described in Table 1. The Flow chart of our model is given in Figure 1, and the nomenclatures in Table 1.

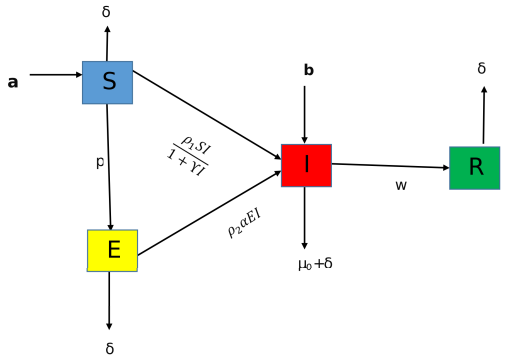

Figure 1. Flow chart of our established Model (1.1).

Table 1. Parameters and their discerption of the model (1.1).

Nomenclature	Representation
S	Susceptible class
E	Exposed class
I	Infected class
R	Recovered class
$\mathbf{N}_0$	Total initial papulation
$\mathbf{N}$	Total population at time t
$\mathbf{b}$	Immigrant to I from E
μ_0	infection death rate
δ	death rate due to natural way
$\mathbf{a}$	Recruitment rate
p	Migration rate from S to E
γ	Saturation value of virus
α	rate at which infection is reducing
ρ_1	contact rate
w	rate at which individual gets ride from infection
ρ_2	infection rate

From Figure 1, we state that **a** is the recruitment rate, and $\frac{\rho_1 SI}{1+\gamma I}$ denoted contact rate. If natural death is involved, then the rate δ and p stands for migration to the exposed class of infection. Thus, the

amount δE is due to natural death and $\rho_2 EI$ denoted the rate of infection which is reduced by rate α. Furthermore, μ_0 is the death rate due to COVID and w denoted recovery rate.

Some essential results, such as disease-free and endemic equilibrium points and basic reproduction numbers, are computed. Additionally, boundness is confirmed. Then, we investigate aforementioned mentioned model for the existence and uniqueness of approximation solutions using Banach and Schauder fixed point theorems. It is noteworthy that the existence theory with piecewise derivatives of fractional orders introduces some novel aspects to such dynamical issues. According to the theory, there is a solution to such physical difficulties. In addition, we provide some results for the numerical interpretation of the system using a numerical scheme. For classic fractional order systems, various numerical tools have proved particularly effective in recent times. For example, in [49], the Range-Kutta approach was employed to solve several fractional order problems. Researchers [50] additionally made use of a revolutionary parameter estimation technique. In [51, 52], a nonstandard numerical approach was utilized to solve fractional order problems. Additionally, improved finite-difference strategies were employed in [53–55] for a distinct set of non-integer order issues. We use genuine data from the sources cited in [56–60] to simulate our results. In this paper, we apply the numerical method to study the numerical analysis of the considered model at different fractional orders.

The manuscript is structured as: Section 1 of our work is devoted to a lengthy introduction. Section 2 contains some essential results that we require in this paper. In addition, some basic results for the proposed model are provided below. In Section 3, we use fixed point theory to develop an existence theory for an approximate solution to the suggested model. The numerical strategy for an approximate solution to the proposed model is covered in Section 4. The Section 5 is dedicated to graphical representations of our findings. Finally, Section 6 provides a quick conclusion and discussion of the numerical results.

2. Elementary results

In the section, we give some fundamental results from fractional calculus which we need throughout this work. Additionally, some basic results for our proposed model are given here.

Definition 2.1. *[42] If* Ω *be differentiable function with* $\mathrm{r} > 0$*, then the classical and fractional order piecewise integration is defined as follows:*

$$ {}_0^{PC}\mathbb{I}_t^{\mathrm{r}}\Omega(t) = \begin{cases} \displaystyle\int_0^{t_1} \Omega(\eta)d\eta, \;\; 0 < t \leq t_1, \\ \displaystyle\frac{1}{\Gamma(\mathrm{r})}\int_{t_1}^{t} (t-\eta)^{\mathrm{r}-1}\Omega(\eta)d(\eta), \;\; t_1 < t \leq T, \end{cases} $$

where ${}_0^{PC}\mathbb{I}_t$ *stands for classical integration in* $0 < t \leq t_1$ *and represents the Riemann-Liouville integration in* $t_1 < t \leq T$.

Definition 2.2. *[42] Let* $0 < \mathrm{r} \leq 1$ *and if* $\Omega \in C[0, T]$ *be differentiable, then the classical and fractional order piecewise derivative is defined as follows:*

$$ {}_0^{PCC}\mathbb{D}_t^{\mathrm{r}}\Omega(t) = \begin{cases} \Omega'(t), \;\; 0 < t \leq t_1, \\ {}_0^{\mathrm{C}}\mathbb{D}_t^{\mathrm{r}}\Omega(t), \;\; t_1 < t \leq T. \end{cases} $$

Lemma 2.3. *[42] Let $\Omega \in L[0,T] \cap C[0,T]$ and $g \in L[0,T]$, then the solution of the given problem*

$$ {}_0^{PCC}\mathbb{D}_t^{\mathrm{r}}\Omega(t) = g(t), \quad 0 < \mathrm{r} \leq 1 $$

is derived as

$$ \Omega(t) = \begin{cases} \Omega_0 + \displaystyle\int_0^t g(\eta)d\eta, \ 0 < t \leq t_1, \\ \Omega(t_1) + \dfrac{1}{\Gamma(\mathrm{r})}\displaystyle\int_{t_1}^t (t-\eta)^{\mathrm{r}-1} g(\eta)d(\eta), \quad t_1 < t \leq t_2. \end{cases} $$

2.1. Some fundamental results about the model (1.1)

Here, we provide some basic results about the model (1.1). The feasible region and boundedness of the proposed model is given in Remark 2.4, as performed in [60].

Remark 2.4. *Let* $\mathbf{N}$ *be the total papulation at any time t, we have*

$$ \mathbf{N} = S + E + I + R. \tag{2.1} $$

Taking derivative of (2.1) *w.r.t 't', and using model* (1.1)*, we get*

$$ {}_0^{PCC}\mathbb{D}_t^{\mathrm{r}}\mathbf{N}(t) \leq \mathbf{a} - \delta\mathbf{N}. \tag{2.2} $$

On solving (2.2) *and taking $t \to \infty$, we get*

$$ \mathbf{N} \leq \frac{\mathbf{a}}{\delta}. $$

Hence, the feasible region is described as

$$ \Phi = \{(S,E,I,R) \in \mathbb{R}_+^4 : \mathbf{N} \leq \frac{\mathbf{a}}{\delta}\}. $$

Hence, the solution is bounded and inside the region is given by Φ.

Putting the left hand sides of model (1.1) equal to zero and solving the equations, the disease free equilibrium is obtained as follows:

$$ \mathbb{E}^0 = (S^0, E^0, 0, 0) = \left(\frac{\mathbf{a}}{(\delta+p)}, \frac{\mathbf{a}p}{\delta(\delta+p)}, 0, 0\right). $$

In the same line, we also compute the endemic equilibria as follows:

$$ \begin{aligned} S^*(t) &= \frac{\mathbf{a}(1+\gamma I^*)}{\rho_1 I^* + (\delta+p)(1+\gamma I^*)} \\ E^*(t) &= \frac{p\mathbf{a}(1+\gamma I^*)}{(\rho_1 I^* + (\delta+p)(1+\gamma I^*))(\delta + \rho_2 \alpha I^*)} \\ R^*(t) &= \frac{wI^*}{\delta}. \end{aligned} $$

Furthermore, the threshold number $\mathbf{R}_0$ is computed by taking the second and third equation of (1.1), from which we have the following:

$$\mathbf{F} = \begin{bmatrix} \frac{\rho_1 SI}{1+\gamma I} + \rho_2 \alpha EI \\ 0 \end{bmatrix} \text{ and } \mathbf{V} = \begin{bmatrix} (\delta + \mu_0 + w - \mathbf{b})I \\ pS - \delta E \end{bmatrix}.$$

Jacobian of $\mathbf{F}$ and $\mathbf{V}$ at disease free equilibrium are given by

$$J(\mathbf{F}) = \begin{pmatrix} \rho_1 S^0 + \rho_2 \alpha E^0 & 0 \\ 0 & 0 \end{pmatrix} \text{ and } J(\mathbf{V}) = \begin{pmatrix} \delta + \mu_0 + w - \mathbf{b} & 0 \\ 0 & \delta \end{pmatrix}.$$

Additionally, one has

$$\mathbf{V}^{-1} = \begin{bmatrix} \frac{1}{\delta+\mu_0+w-\mathbf{b}} & 0 \\ 0 & \frac{1}{\delta} \end{bmatrix}$$

$$\mathbf{FV}^{-1} = \begin{bmatrix} \frac{\rho_1 S^0 + \rho_2 \alpha E^0}{\delta+\mu_0+w-\mathbf{b}} & 0 \\ 0 & 0 \end{bmatrix}.$$

Hence, $\mathbf{R}_0$ is obtained as follows:

$$\mathbf{R}_0 = \frac{\rho_1 \mathbf{a}\delta + \rho_2 \alpha \mathbf{a}}{\delta(\delta + p)(\delta + \mu_0 + w - \mathbf{b})}. \tag{2.3}$$

In Figure 2, we present a $3D$ profile of $\mathbf{R}_0$ for some specific values, as given in Table 2.

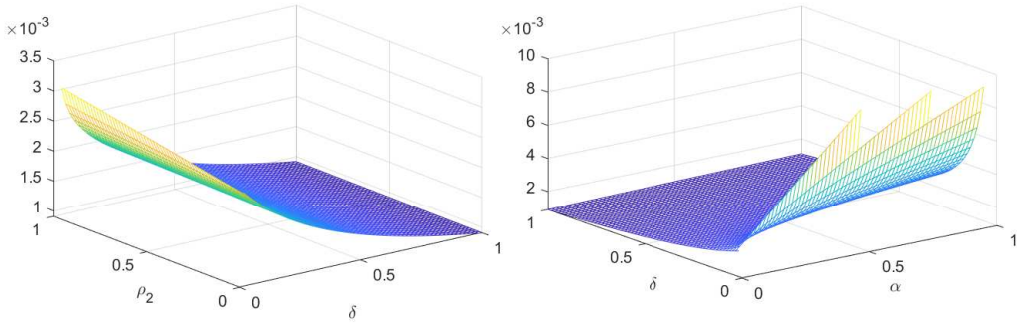

Figure 2. 3D profile of $\mathbf{R}_0$ computed in (2.3).

Table 2. Numerical values of the nomenclatures of the model.

Nomenclature	Numerical value
S	217.342565 in millions [56]
E	100 in million (assumed)
I	1.386348 in million [56]
R	1.271087 in million [56]
$\mathbf{b}$	0.135 (assumed) day^{-1}
μ_0	0.19 [56] day^{-1}
δ	0.000065 [56] day^{-1}
$\mathbf{a}$	1.43 [60] day^{-1}
p	0.45 day^{-1} [60]
γ	0.00019 [60] day^{-1}
α	0.0008601 [60] day^{-1}
ρ_1	0.10 [60] day^{-1}
w	0.98 [60] day^{-1}
ρ_2	0.020 [60] day^{-1}

3. Existence theory

In this section, we will develop the existence and uniqueness results for the solution of the proposed model (1.1). To proceed, let $G : [0, T] \times \mathbb{R} \to \mathbb{R}$ be a nonlinear continuous function, then the solution according to Lemma 2.3 of

$$\begin{aligned} {}_0^{PCC}\mathbb{D}_t^{\mathrm{r}}\Omega(t) &= G(t, \Omega), \ \ 0 < \mathrm{r} \leq 1, \\ \Omega(0) &= \Omega_0 \end{aligned} \tag{3.1}$$

is given as

$$\Omega(t) = \begin{cases} \Omega_0 + \int_0^t G(\eta, \Omega(\eta))d\eta, \ 0 < t \leq t_1, \\ \Omega(t_1) + \frac{1}{\Gamma(\mathrm{r})}\int_{t_1}^{t_2}(t-\eta)^{\mathrm{r}-1}G(\eta, \Omega(\eta))d(\eta), \ \ t_1 < t \leq t_2, \end{cases} \tag{3.2}$$

where

$$\Omega(t) = \begin{pmatrix} S(t) \\ E(t) \\ I(t) \\ R(t) \end{pmatrix}, \quad \Omega_0 = \begin{pmatrix} S_0 \\ E_0 \\ I_0 \\ R_0 \end{pmatrix}, \quad \Omega(t_1) = \begin{pmatrix} S(t_1) \\ E(t_1) \\ I(t_1) \\ R(t_1) \end{pmatrix}, \quad G(t, \Omega(t)) = \begin{cases} G_1(t, \Omega(t)) = \begin{cases} G_1(\Omega, t), 0 < t < t_1, \\ G_1(\Omega, t), t_1 < t \leq t_2, \end{cases} \\ G_2(t, \Omega(t)) = \begin{cases} G_2(\Omega, t), 0 < t < t_1, \\ G_2(\Omega, t), t_1 < t \leq t_2, \end{cases} \\ G_3(t, \Omega(t)) = \begin{cases} G_3(\Omega, t), 0 < t < t_1, \\ G_3(\Omega, t), t_1 < t \leq t_2, \end{cases} \\ G_4(t, \Omega(t)) = \begin{cases} G_4(\Omega, t), 0 < t < t_1, \\ G_4(\Omega, t), t_1 < t \leq t_2. \end{cases} \end{cases} \tag{3.3}$$

Let $\infty > t_2 \geq t > t_1 > 0$, with space described by $\mathbb{E} = C[0,T]\times C[0,T]\times C[0,T]\times C[0,T]$ endowed with norm

$$||\Omega|| = \max_{t\in[0,T]} |\Omega(t)|.$$

The given hypothesis will hold.

(C1) Let $\mathbb{L}_G > 0$, such that $\Omega,\ \bar{\Omega} \in \mathbb{E}$, then

$$|G(t,\Omega) - G(t,\bar{\Omega})| \leq \mathbb{L}_G|\Omega - \bar{\Omega}|.$$

(C2) If $C_G > 0$, and $M_G > 0$, then

$$|G(t,\Omega(t))| \leq C_G|\Omega| + M_G.$$

Theorem 3.1. *Under the hypothesis* $(C1),(C2)$, *and if there exists a closed bounded subset*

$$\mathbb{B} = \{\Omega \in \mathbb{E} :\ ||\Omega|| \leq R_{1,2},\ R_{1,2} > 0\},$$

where

$$R_{1,2} \geq \max\begin{cases} \dfrac{|\Omega_0| + t_1M_G}{1 - t_1C_G},\ 0 < t \leq t_1, \\ \dfrac{|\Omega(t_1)|\Gamma(\mathrm{r}+1) + T^{\mathrm{r}}M_G}{(\Gamma(\mathrm{r}+1) - T^{\mathrm{r}}C_G},\ t_1 < t \leq t_2, \end{cases}$$

then the problem (3.1) *has at least on solution. Consequently the proposed model* (1.1) *has at least one solution.*

Proof. Let $\mathbb{B}$ of $\mathbb{E}$ as follows:

$$\mathbb{B} = \{\Omega \in \mathbb{E} :\ ||\Omega|| \leq R_{1,2},\ R_{1,2} > 0\}.$$

Here, we describe the operator by $\mathbb{T} : \mathbb{B} \to \mathbb{B}$ as follows:

$$\mathbb{T}(\Omega) = \begin{cases} \Omega_0 + \displaystyle\int_0^t G(\eta,\Omega(\eta))d\eta,\ 0 < t \leq t_1, \\ \Omega(t_1) + \dfrac{1}{\Gamma\mathrm{r}}\displaystyle\int_{t_1}^{t_2}(t-\eta)^{\sigma-1}G(\eta,\Omega(\eta))d(\eta),\ \ t_1 < t \leq t_2. \end{cases} \tag{3.4}$$

For $\Omega \in \mathbb{B}$, we have the following:

$$\begin{aligned} |\mathbb{T}(\Omega)(t)| &\leq \begin{cases} |\Omega_0| + \displaystyle\int_0^{t_1}|G(\eta,\Omega(\eta))|d\eta, \\ |\Omega(t_1)| + \dfrac{1}{\Gamma(\mathrm{r})}\displaystyle\int_{t_1}^{t_2}(t-\eta)^{\mathrm{r}-1}|G(\eta\Omega(\eta))|d(\eta), \end{cases} \\ &\leq \begin{cases} |\Omega_0| + \displaystyle\int_0^{t_1}[C_G|\Omega| + M_G]d\eta, \\ |\Omega(t_1)| + \dfrac{1}{\Gamma(\mathrm{r})}\displaystyle\int_{t_1}^{t_2}(t-\eta)^{\mathrm{r}-1}[C_G|\Omega| + M_G]d(\eta), \end{cases} \end{aligned}$$

$$\leq \begin{cases} |\Omega_0| + t_1[C_G R_{1,2} + M_G] \leq R_{1,2}, \ 0 < t \leq t_1, \\ |\Omega(t_1)| + \dfrac{T^{\mathrm{r}}}{\Gamma(\mathrm{r}+1)}[C_G R_{1,2} + M_G] \leq R_{1,2}, \ t_1 < t \leq t_2, \end{cases}$$

where for $t_1 < t <\leq t_2$, we put $|(t_1 - \eta)^{\mathrm{r}} - (t_2 - \eta)^{\mathrm{r}}| \leq T^{\mathrm{r}}$. Hence, we have that $\|\mathbb{T}(\Omega)\| \leq R_{1,2}$ which yields that $\mathbb{T}(\mathbb{B}) \subset \mathbb{B}$. Thus, $\mathbb{T}$ maps bounded set to bounded. Thus, $\mathbb{T}$ is a bounded operator since G is continuous function. Therefore, $\mathbf{T}$ is also a continuous operator. Additionally, take $t_n > t_m \in [0, t_1]$, then

$$\begin{aligned} |\mathbb{T}(\Omega)(t_n) - \mathbb{T}(\Omega)(t_m)| &= \left| \int_0^{t_n} G(\eta, \Omega(\eta))d\eta - \int_0^{t_m} G(\eta, \Omega(\eta))d\eta \right| \\ &\leq \int_{t_m}^{t_n} |G(\eta, \Omega(\eta))|d\eta \\ &\leq \int_{t_m}^{t_n} [C_G|\Omega| + M_G]d\eta \\ &\leq (C_G R_{1,2} + M_G)[t_n - t_m]. \end{aligned} \tag{3.5}$$

From (3.5), we see that $t_n \to t_m$, then

$$|\mathbb{T}(\Omega)(t_n) - \mathbb{T}(\Omega)(t_m)| \to 0, \text{ as } t_n \to t_m.$$

Additionally, $\mathbb{T}$ is a bounded operator. Therefore,

$$\|\mathbb{T}(\Omega)(t_n) - \mathbb{T}(\Omega)(t_m)\| \to 0, \text{ as } t_n \to t_m.$$

Hence, in this case, $\mathbb{T}$ is equi-continuous in this case. Furthermore, for $t_n > t_m \in (t_1, T]$, consider the following:

$$\begin{aligned} |\mathbb{T}(\Omega)(t_n) - \mathbb{T}(\Omega)(t_m)| &= \left| \frac{1}{\Gamma(\mathrm{r})} \int_0^{t_n} (t_n - \eta)^{\mathrm{r}-1} G(\eta, \Omega(\eta))d\eta - \frac{1}{\Gamma(\mathrm{r})} \int_0^{t_m} (t_m - \eta)^{\mathrm{r}-1} G(\eta, \Omega(\eta))d\eta \right| \\ &\leq \frac{1}{\Gamma(\mathrm{r})} \int_0^{t_m} [(t_m - \eta)^{\mathrm{r}-1} - (t_n - \eta)^{\mathrm{r}-1}]|G(\eta, \Omega(\eta))|d\eta \\ &+ \frac{1}{\Gamma(\mathrm{r})} \int_{t_m}^{t_n} (t_n - \eta)^{\mathrm{r}-1} |G(\eta, \Omega(\eta))|d\eta \\ &\leq \frac{1}{\Gamma(\mathrm{r})} \Big[\int_0^{t_m} [(t_m - \eta)^{\mathrm{r}-1} - (t_n - \eta)^{\mathrm{r}-1}]d\eta \\ &+ \int_{t_m}^{t_n} (t_n - \eta)^{\mathrm{r}-1} d\eta \Big] (C_G|\Omega| + M_G) \\ &\leq \frac{(C_G R_{1,2} + M_G)}{\Gamma(\mathrm{r}+1)} [t_n^{\mathrm{r}} - t_m^{\mathrm{r}} + 2(t_n - t_m)^{\mathrm{r}}]. \end{aligned} \tag{3.6}$$

Furthermore, from (3.6), we see that

$$|\mathbb{T}(\Omega)(t_n) - \mathbb{T}(\Omega)(t_m)| \to 0, \text{ as } t_m \to t_n.$$

Additionally, $\mathbb{T}$ is bounded over $(t_1, T]$ so is uniformly continuous. Hence,

$$||\mathbb{T}(\Omega)(t_n) - \mathbb{T}(\Omega)(t_m)|| \to 0, \text{ as } t_n \to t_m.$$

Therefore, $\mathbb{T}$ is equi-continuous in the $(t_1, t_2]$ interval. Hence $\mathbb{T}$ is an equi-continuous mapping over $[0, t_1] \cup (t_1, t_2]$. Thus, $\mathbb{T}$ is a relatively compact operator. By using the Arzelá-Ascoli theorem, the operator $\mathbb{T}$ is completely continuous. Hence, the concerned problem (3.1) and the proposed model (1.1) have at least one solution.

□

Theorem 3.2. *Inview of Hypothesis* $(C1)$*, the problem* (3.1) *has a unique solution if* $\max\left\{T\mathbb{L}_G, \frac{T^{\mathrm{r}}}{\Gamma(\mathrm{r}+1)}\mathbb{L}_G\right\} < 1$. *Consequently, the proposed model* (1.1) *has a unique solution.*

Proof. If $\mathbb{T} : \mathbb{E} \to \mathbb{E}$ can be described as follows:

$$\mathbb{T}(\Omega) = \begin{cases} \Omega_0 + \displaystyle\int_0^t G(\eta, \Omega(\eta))d\eta, \ 0 < t \leq t_1, \\ \Omega(t_1) + \dfrac{1}{\Gamma \mathrm{r}} \displaystyle\int_{t_1}^{t_2} (t-\eta)^{\sigma-1} G(\eta, \Omega(\eta))d(\eta), \ \ t_1 < t \leq t_2. \end{cases}$$

Then $\Omega, \ \bar{\Omega} \in \mathbb{E}$, over $[0, t_1]$, one has

$$\begin{aligned} ||\mathbb{T}(\Omega) - \mathbb{T}(\bar{\Omega})|| &= \max_{t\in[0,t_1]} \left| \int_0^{t_1} G(\eta, \Omega(\eta))d\eta - \int_0^{t_1} G(\eta, \bar{\Omega}(\eta))d\eta \right| \\ &\leq T\mathbb{L}_G||\Omega - \bar{\Omega}||. \end{aligned} \tag{3.7}$$

From (3.7), we have

$$||\mathbb{T}(\Omega) - \mathbb{T}(\bar{\Omega})|| \leq T\mathbb{L}_G||\Omega - \bar{\Omega}||. \tag{3.8}$$

By the same fashion for $t \in (t_1, t_2]$, we have

$$\begin{aligned} ||\mathbb{T}(\Omega) - \mathbb{T}(\bar{\Omega})|| &= \max_{t\in(t_1,t_2]} \left| \frac{1}{\Gamma(\mathrm{r})} \int_{t_1}^{t_2} (t-\eta)^{\mathrm{r}-1} G(\eta, \Omega(\eta))d\eta - \frac{1}{\Gamma(\mathrm{r})} \int_{t_1}^{t_2} (t-\eta)^{\mathrm{r}-1} G(\eta, \bar{\Omega}(\eta))d\eta \right| \\ &\leq \frac{T^{\mathrm{r}}}{\Gamma(\mathrm{r}+1)}\mathbb{L}_G||\Omega - \bar{\Omega}||. \end{aligned} \tag{3.9}$$

From (3.9), we have

$$||\mathbb{T}(\Omega) - \mathbb{T}(\bar{\Omega})|| \leq \frac{T^{\mathrm{r}}}{\Gamma(\mathrm{r}+1)}\mathbb{L}_G||\Omega - \bar{\Omega}||. \tag{3.10}$$

Hence, from (3.8) and (3.10), we see that $\mathbb{T}$ is a contraction operator. Hence, (3.1) has a unique solution. Consequently, our proposed model (1.1) has a unique solution. □

4. Numerical scheme

Here, for the conduction of numerical results and for the proposed model (1.1), we construct a numerical method for the two sub-intervals of $[0, t_2]$. The numerical scheme for the piecewise problem is like an integer order numerical scheme, as established in [42]. Using the piece-wise integral form of 1.1, the classical and Caputo format is as follows:

$$
\begin{aligned}
S(t)) &= \begin{cases} S_0 + \displaystyle\int_0^{t_1} G_1(\eta,)d\eta, \;\; 0 < t \le t_1, \\ S(t_1) + \dfrac{1}{\Gamma(\mathrm{r})} \displaystyle\int_{t_1}^{t_2} (t-\eta)^{\mathrm{r}-1} G_1(\eta)d\eta, \;\; t_1 < t \le t_2, \end{cases}, \\
E(t)) &= \begin{cases} E_0 + \displaystyle\int_0^{t_1} G_2(\eta,)d\eta, \;\; 0 < t \le t_1, \\ E(t_1) + \dfrac{1}{\Gamma(\mathrm{r})} \displaystyle\int_{t_1}^{t_2} (t-\eta)^{\mathrm{r}-1} G_2(\eta)d\eta, \;\; t_1 < t \le t_2, \end{cases}, \\
I(t)) &= \begin{cases} I_0 + \displaystyle\int_0^{t_1} G_3(\eta,)d\eta, \;\; 0 < t \le t_1, \\ I(t_1) + \dfrac{1}{\Gamma(\mathrm{r})} \displaystyle\int_{t_1}^{t_2} (t-\eta)^{\mathrm{r}-1} G_3(\eta)d\eta, \;\; t_1 < t \le t_2, \end{cases}, \\
\mathbb{U}(t)) &= \begin{cases} R_0 + \displaystyle\int_0^{t_1} G_4(\eta,)d\eta, \;\; 0 < t \le t_1, \\ R(t_1) + \dfrac{1}{\Gamma(\mathrm{r})} \displaystyle\int_{t_1}^{t_2} (t-\eta)^{\mathrm{r}-1} G_4(\eta)d\eta, \;\; t_1 < t \le t_2. \end{cases}
\end{aligned} \tag{4.1}
$$

First, we construct the technique for the first equation of system (4.1), and the same procedure will be repeated for the remaining equations. At $t = t_{n+1}$, we have

$$
S(t_{n+1})) = \begin{cases} S_0 + \displaystyle\int_0^{t_1} G_1(\Omega, \eta)d\eta, 0 < t \le t_1, \\ S(t_1) + \dfrac{1}{\Gamma(\mathrm{r})} \displaystyle\int_{t_1}^{t_{n+1}} (t-\eta)^{\mathrm{r}-1} G_1(S, E, I, R, \eta)d\eta, \;\; t_1 < t \le t_2, \end{cases} \tag{4.2}
$$

We express Eq (4.2) in the Newton interpolation formula given in [42] as

$$S(t_{n+1}) = \begin{cases} S_0 + \begin{cases} \sum_{k=2}^{i} \Big[\frac{5}{12} G_1(S^{k-2}, E^{k-2}, I^{k-2}, R^{k-2}, t_{k-2}) \mathrm{r}t \\ - \frac{4}{3} G_1(S^{k-1}, E^{k-1}, I^{k-1}, R^{k-1}, t_{k-1}) \mathrm{r}t + G_1(S^k, E^k, I^k, R^k, t_k) \Big], \end{cases} \\ S(t_1) + \begin{cases} \frac{(\mathrm{r}t)^{\mathrm{r}-1}}{\Gamma(\mathrm{r}+1)} \sum_{k=i+3}^{n} \Big[G_1(S^{k-2}, E^{k-2}, I^{k-2}, R^{k-2}, t_{k-2}) \Big] \Pi \\ + \frac{(\mathrm{r}t)^{\mathrm{r}-1}}{\Gamma(\mathrm{r}+2)} \sum_{k=i+3}^{n} \Big[G_1(S^{k-1}, E^{k-1}, I^{k-1}, R^{k-1}, t_{k-1}) \\ - G_1(S^{k-2}, E^{k-2}, I^{k-2}, R^{k-2}, t_{k-2}) \Big] \Lambda \\ + \frac{\mathrm{r}(\mathrm{r}t)^{\mathrm{r}-1}}{2\Gamma(\mathrm{r}+3)} \sum_{k=i+3}^{n} \Big[G_1(S^k, E^k, I^k, R^k, t_k) - 2G_1(S^{k-1}, E^{k-1}, I^{k-1}, R^{k-1}, t_{k-1}) \\ + G_1(S^{k-2}, E^{k-2}, I^{k-2}, R^{k-2}, t_{k-2}) \Big] \Xi. \end{cases} \end{cases} \tag{4.3}$$

For the rest of the three equations, we can write the Newton interpolation scheme as follows:

$$E(t_{n+1}) = \begin{cases} E_0 + \begin{cases} \sum_{k=2}^{i} \Big[\frac{5}{12} G_2(S^{k-2}, E^{k-2}, I^{k-2}, R^{k-2}, t_{k-2}) \mathrm{r}t \\ - \frac{4}{3} G_2(S^{k-1}, E^{k-1}, I^{k-1}, R^{k-1}, t_{k-1}) \mathrm{r}t + G_2(S^k, E^k, I^k, R^k, t_k) \Big], \end{cases} \\ E(t_1) + \begin{cases} \frac{(\mathrm{r}t)^{\mathrm{r}-1}}{\Gamma(\mathrm{r}+1)} \sum_{k=i+3}^{n} \Big[G_2(S^{k-2}, E^{k-2}, I^{k-2}, R^{k-2}, t_{k-2}) \Big] \Pi \\ + \frac{(\mathrm{r}t)^{\mathrm{r}-1}}{\Gamma(\mathrm{r}+2)} \sum_{k=i+3}^{n} \Big[G_2(S^{k-1}, E^{k-1}, I^{k-1}, R^{k-1}, t_{k-1}) \\ - G_2(S^{k-2}, E^{k-2}, I^{k-2}, R^{k-2}, t_{k-2}) \Big] \Lambda \\ + \frac{\mathrm{r}(\mathrm{r}t)^{\mathrm{r}-1}}{2\Gamma(\mathrm{r}+3)} \sum_{k=i+3}^{n} \Big[G_2(S^k, E^k, I^k, R^k, t_k) - 2G_2(S^{k-1}, E^{k-1}, I^{k-1}, R^{k-1}, t_{k-1}) \\ + G_2(S^{k-2}, E^{k-2}, I^{k-2}, R^{k-2}, t_{k-2}) \Big] \Xi \end{cases} \end{cases}, \tag{4.4}$$

$$I(t_{n+1}) = \begin{cases} I_0 + \begin{cases} \sum_{k=2}^{i} \Big[\frac{5}{12} G_3(S^{k-2}, E^{k-2}, I^{k-2}, R^{k-2}, t_{k-2}) \mathrm{r}t \\ - \frac{4}{3} G_3(S^{k-1}, E^{k-1}, I^{k-1}, R^{k-1}, t_{k-1}) \mathrm{r}t + G_3(S^{k}, E^{k}, I^{k}, R^{k}, t_{k}) \Big], \end{cases} \\ I(t_1) + \begin{cases} \frac{(\mathrm{r}t)^{\mathrm{r}-1}}{\Gamma(\mathrm{r}+1)} \sum_{k=i+3}^{n} \Big[G_3(S^{k-2}, E^{k-2}, I^{k-2}, R^{k-2}, t_{k-2}) \Big] \Pi \\ + \frac{(\mathrm{r}t)^{\mathrm{r}-1}}{\Gamma(\mathrm{r}+2)} \sum_{k=i+3}^{n} \Big[G_3(S^{k-1}, E^{k-1}, I^{k-1}, R^{k-1}, t_{k-1}) \\ - G_3(S^{k-2}, E^{k-2}, I^{k-2}, R^{k-2}, t_{k-2}) \Big] \Lambda \\ + \frac{\mathrm{r}(\mathrm{r}t)^{\mathrm{r}-1}}{2\Gamma(\mathrm{r}+3)} \sum_{k=i+3}^{n} \Big[G_3(S^{k}, E^{k}, I^{k}, R^{k}, t_{k}) - 2G_3(S^{k-1}, E^{k-1}, I^{k-1}, R^{k-1}, t_{k-1}) \\ + G_3(S^{k-2}, E^{k-2}, I^{k-2}, R^{k-2}, t_{k-2}) \Big] \Xi \end{cases} \end{cases} \tag{4.5}$$

$$R(t_{n+1}) = \begin{cases} R_0 + \begin{cases} \sum_{k=2}^{i} \Big[\frac{5}{12} G_4(S^{k-2}, E^{k-2}, I^{k-2}, R^{k-2}, t_{k-2}) \mathrm{r}t \\ - \frac{4}{3} G_4(S^{k-1}, E^{k-1}, I^{k-1}, R^{k-1}, t_{k-1}) \mathrm{r}t + G_4(S^{k}, E^{k}, I^{k}, R^{k}, t_{k}) \Big], \end{cases} \\ R(t_1) + \begin{cases} \frac{(\mathrm{r}t)^{\mathrm{r}-1}}{\Gamma(\mathrm{r}+1)} \sum_{k=i+3}^{n} \Big[G_4(S^{k-2}, E^{k-2}, I^{k-2}, R^{k-2}, t_{k-2}) \Big] \Pi \\ + \frac{(\mathrm{r}t)^{\mathrm{r}-1}}{\Gamma(\mathrm{r}+2)} \sum_{k=i+3}^{n} \Big[G_4(S^{k-1}, E^{k-1}, I^{k-1}, R^{k-1}, t_{k-1}) \\ - G_4(S^{k-2}, E^{k-2}, I^{k-2}, R^{k-2}, t_{k-2}) \Big] \Lambda \\ + \frac{\mathrm{r}(\mathrm{r}t)^{\mathrm{r}-1}}{2\Gamma(\mathrm{r}+3)} \sum_{k=i+3}^{n} \Big[G_4(S^{k}, E^{k}, I^{k}, R^{k}, t_{k}) - 2G_4(S^{k-1}, E^{k-1}, I^{k-1}, R^{k-1}, t_{k-1}) \\ + G_4(S^{k-2}, E^{k-2}, I^{k-2}, R^{k-2}, t_{k-2}) \Big] \Xi \end{cases} \end{cases}, \tag{4.6}$$

where $\Pi = (n-k+1)^{\mathrm{r}} - (n-j)^{\mathrm{r}}$, $\Lambda = (n-k+1)^{\mathrm{r}}(n-k+3+2\mathrm{r}) - (n-k)(n-k+3+3\mathrm{r})$,

$\Xi = [(n-k+1)^{\alpha}(2(n-k)^2+(3\alpha+10)(n-k)+2\alpha^2+9\alpha+12) - (n-k)^{\alpha}(2(n-k)^2+((5\alpha+10)(n-k)+6\alpha^2+18\alpha+12)$.

5. Numerical simulation

In this section, we present the numerical simulation in Figures 3–10 using the obtained scheme of Newton polynomials of classical and piecewise derivative concepts. We divide the whole interval

into two sub-intervals and check the first interval for the integer order derivative, while the second a interval is tested on different fractional orders in the sense of Caputo derivative by using the data given in Table 2.

Figures 3 and 4 represent, the susceptible population, which declines and then becomes stable as the remaining classes increase on both intervals. The single curve is for the first interval and it shows integer order classical behavior from $[0, t_1] = [0, 20]$, while the four different curves show the global order derivative behavior on $[t_1, t_2] = [20, 80]$. In Figure 4, the intervals are slightly increased and shows a similar behavior.

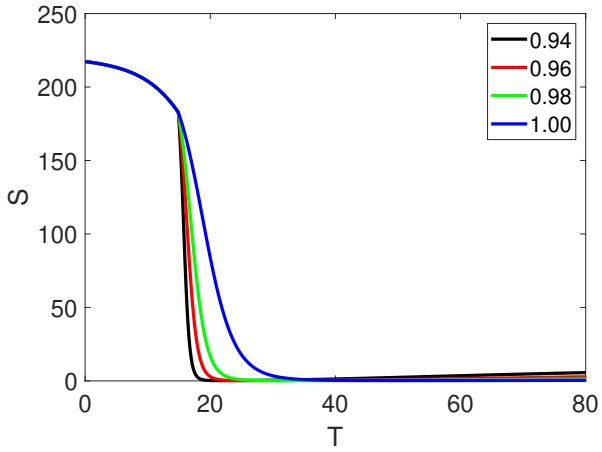

Figure 3. Piecewise representation of approximate solution for S for classical derivative on $[0, t_1]$ and fractional order derivative on $[t_1, t_2]$ of order r.

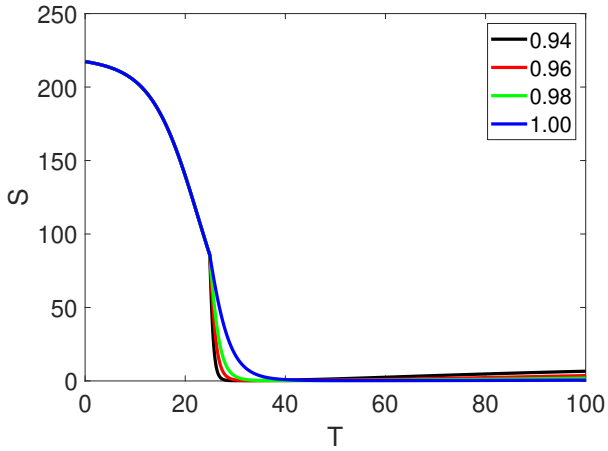

Figure 4. Piecewise representation of approximate solution for S for classical derivative on $[0, t_1]$ and fractional order derivative on $[t_1, t_2]$ of order r.

Next, Figures 5 and 6 represent the exposed population, which grows up and then becomes stable as the remaining two classes decline on both intervals. The single curve is for the first interval and it shows classical order dynamics on $[0, t_1]$, while the four different curves show the fractional Caputo order derivative behavior on $[t_1, t_2]$. In Figure 6, the time interval is $[0, 100]$, showing similar dynamics.

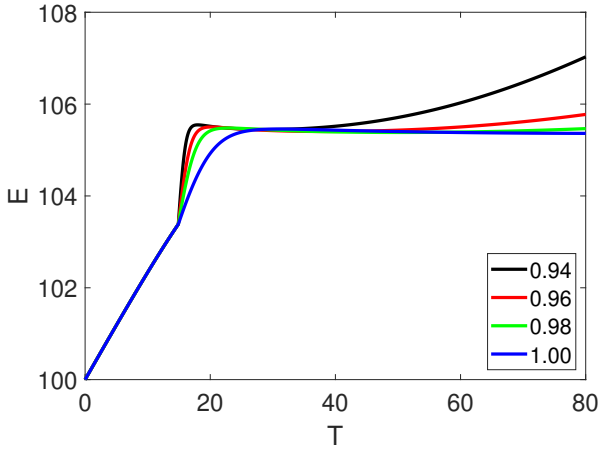

Figure 5. Piecewise representation of approximate solution for E for classical derivative on $[0, t_1]$ and fractional order derivative on $[t_1, t_2]$ of order r.

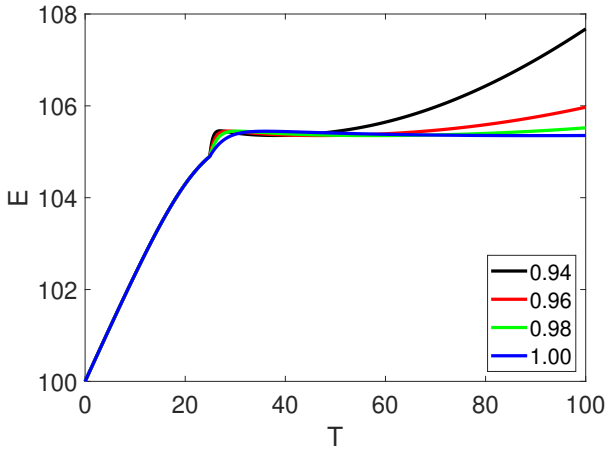

Figure 6. Piecewise representation of approximate solution for E for classical derivative on $[0, t_1]$ and fractional order derivative on $[t_1, t_2]$ of order r.

Furthermore, Figures 7 and 8 show the infected population, which grows up and reaches its peak value, and then declines towards the convergent point. The first shows the integer order derivative, while the other show, the fractional Caputo derivative behavior on different fractional orders. In Figure 8, the time interval is changed, showing similar dynamics.

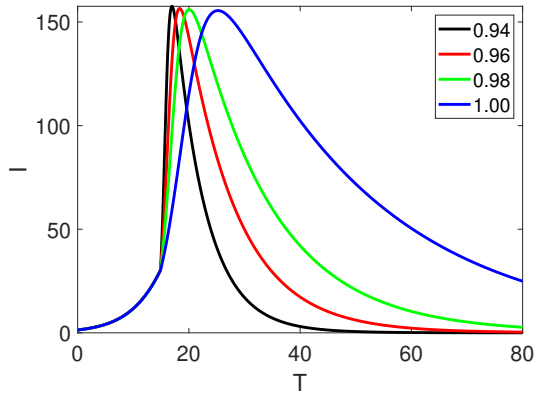

Figure 7. Piecewise representation of approximate solution for I for classical derivative on $[0, t_1]$ and fractional order derivative on $[t_1, t_2]$ of order r.

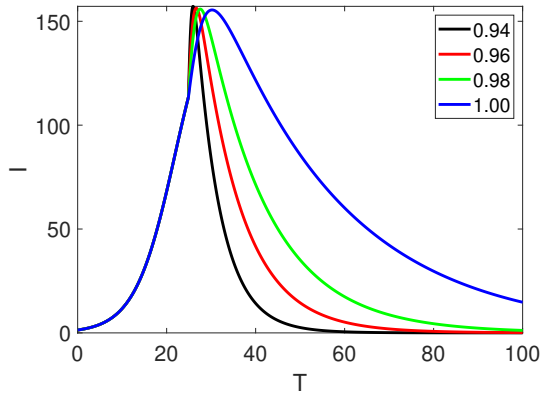

Figure 8. Piecewise representation of approximate solution for I for classical derivative on $[0, t_1]$ and fractional order derivative on $[t_1, t_2]$ of order r.

The dynamics of the recovered population are shown in Figures 9 and 10, which indicate a sluggish increase at the first interval of the integer order, followed by a fast increase that leads to the population's stable value at the convergent point. The fractional Caputo order derivative dynamics are represented by the second interval, whilst the integer order derivative is represented by the first interval. The time interval is extended and the same dynamical behavior is displayed in Figure 10.

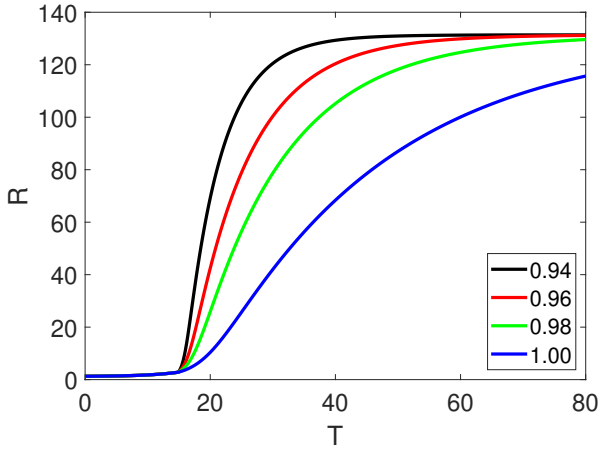

Figure 9. Piecewise representation of approximate solution for R for classical derivative on $[0, t_1]$ and fractional order derivative on $[t_1, t_2]$ of order r.

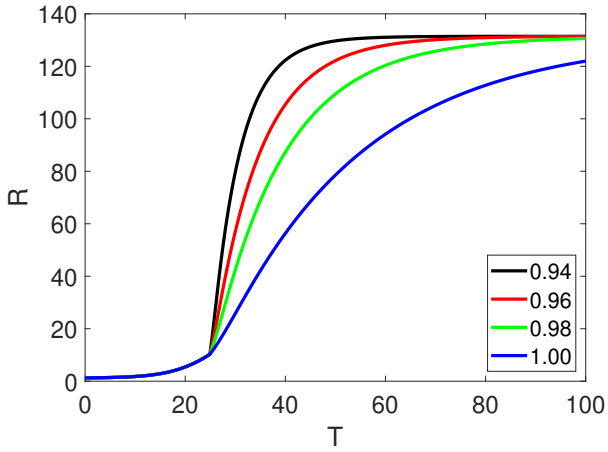

Figure 10. Piecewise representation of approximate solution for R for classical derivative on $[0, t_1]$ and fractional order derivative on $[t_1, t_2]$ of order r.

Here, we compare our results in ordinary form with some actual data for infected patients reported for 200 days in Pakistan, using the source [59] at the specified fractional order. We can see that the simulated findings closely match those of actual data. This phenomenon shows that our plan and numerical analysis are valid. Additionally, we evaluated our numerical results with those of genuine data for Pakistan from the 1st March 2021 to the 15th September 2021, as provided by [60] in Figure 11.

$$\{4, 4, 5, 5, 5, 5, 5, 6, 15, 17, 18, 19, 19, 31, 51, 182, 245, 331, 439, 485, 629, 758, 856, 962, 1034, 1171, 1139,$$
$$1454.1554, 1836, 1997, 2262, 2520, 2646, 2899, 3058, 3549, 3735, 3852, 3902, 4162, 4150, 4307, 4362, 4824,$$
$$5143, 5122, 6043, 6742, 7286, 7703, 8479, 8925, 9438, 10103, 10586, 11058, 11747, 11996, 12380, 12900,$$
$$13818, 14498, 14814, 15716, 16370, 17574, 18003, 20267, 21587, 22037, 23268, 25609, 26003, 26230, 27054,$$
$$27904, 29266, 30503, 31775, 32578, 34386, 34642, 36228, 37657, 38150, 38900, 39690, 40358, 40880,$$
$$42687, 47607, 50234, 53300, 56144, 59394, 63400, 57170, 60470, 75053, 78699, 83182, 79700, 84762,$$

85321, 89583, 93233, 97690, 100324, 104648, 105087, 106142, 107733, 107270, 107607, 107460, 107784,
106023, 106775, 106361, 108100, 108466, 103543, 95388, 95241, 95219, 73536, 60234, 57668,
53431, 53333, 52203, 51057, 50080, 94522, 91408, 87345, 86770, 84234, 77418, 77360, 40242,
29274, 29626, 27189, 26191, 25279, 24983, 24941, 24912, 24908, 24935, 24827, 20597, 19230, 18253,
17573, 17548, 17555, 17588, 17103, 16229, 16685, 16001, 13706, 13385, 12464, 11697, 11542, 10378, 10446,
9940, 9356, 8739, 8555, 8585, 8500, 8553, 8623, 16014, 8633, 8564, 8512, 8660, 8883, 6020, 6234,
6477, 6545, 5291, 5546, 5979, 5786, 5582, 5525$\Big\}$.

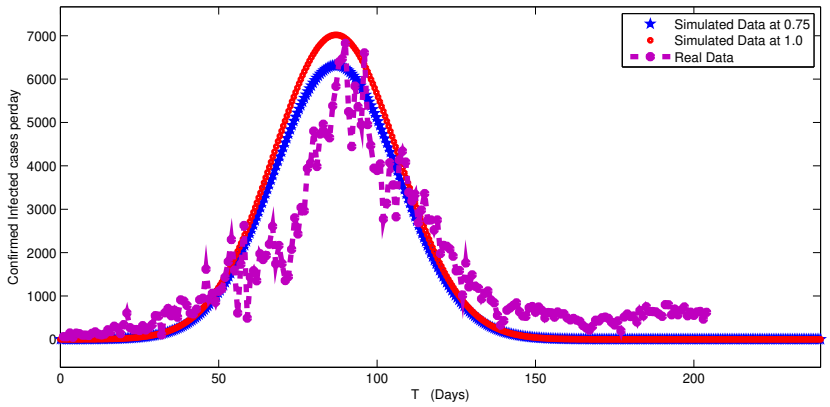

Figure 11. Comparison of per day infected cases with that of simulated data of our proposed model.

Here, we have compared the results of the simulation with real data from the case of the infected class. We see simulated results are closely related. Furthermore, fractional order derivatives maintain a higher degree of freedom and flexibility. Figures 3–10 show the crossover behavior at the indicated positions. Two sets of various fractional orders and time intervals have been used in the numerical simulation of all four compartments. Additionally, the bending effects are also displayed when t_1 is used to describe the dynamics of piecewise derivatives. The physical piecewise concept is more realistic when compared to either classical or traditional fractional order derivatives because abrupt changes cannot be modeled accurately using traditional fractional calculus. Hence, the multi-behaviors of transmission dynamics cannot be properly described via the traditional concept. Hence, the said tools of fractional calculus can be used as a powerful tool to physically interpret various dynamical systems of real world process/problems more comprehensively.

6. Discussion and conclusions

In this study, a model based on piecewise equations with fractional order Caputo derivatives was established. We used the fixed point theory of Schauder and Banach to build the existence theory of the solution of the suggested model. Additionally, we developed a numerical approach based on the Newton interpolation formula. Then, the outcomes were represented graphically using real data for different fractional orders. Additionally, for the aforementioned afflicted individuals, relevant results

have been shown and contrasted with actual data. This is known as crossover behavior because many real-world problems have sudden changes to their state of uniform motion or rest. Traditional fractional or classical derivatives of any kind are ineffective for illustrating this phenomenon. The aforementioned phenomenon is adequately explained by piecewise equations with fractional order derivatives.

Additionally, there was a comparison between the solutions and the integer order solution. The initial interval of the numerical simulation was given in the integer order, whereas the second interval is checked in multiple fractional orders. Both intervals are analyzed on fractional orders in addition to the comparison with the integer order. When abrupt changes in the dynamics of various parameters occur, such an analysis can be utilized to investigate a variety of worldwide occurrences. The crossover issues of both integer and fractional orders can be addressed by this investigation. Finally, we conducted a careful comparison of our results with a few verified facts. Future uses of this form of analysis will involve more complex dynamical problems, such as Mittag-Leffler derivatives and fractal-fractional types. Then, the above model will be investigated in the framework of stochastic fractional order differential equations using singular and non-singular differential operators.

Use of AI tools declaration

The authors declare they have not used Artificial Intelligence (AI) tools in the creation of this article.

Acknowledgements

The authors extend their appreciation to the Deputyship for Research & Innovation, Ministry of Education in Saudi Arabia for funding this research through the project number IFP-IMSIU-2023126. The authors also appreciate the Deanship of Scientific Research at Imam Mohammad Ibn Saud Islamic University (IMSIU) for supporting and supervising this project.

Conflict of interest

The authors declare that they have no any kind of conflict of interest regarding this work.

References

1. World Health Organization (WHO), Naming the coronavirus disease (COVID-19) and the virus that causes it, 2020.
2. D. S. Hui, E. I Azhar, T. A. Madani, F. Ntoumi, R. Kock, O. Dar, et al., The continuing 2019-nCoV epidemic threat of novel coronaviruses to global health-The latest 2019 novel coronavirus outbreak in Wuhan, China, *Int. J. Infect. Dis.*, **91** (2020) 264–266. https://doi.org/10.1016/j.ijid.2020.01.009
3. S. Zhao, Q. Lin, J. Ran, S. S. Musa, G. Yang, W. Wang, et. al, Preliminary estimation of the basic reproduction number of novel coronavirus (2019-nCoV) in China, *Int. J. Infect. Dis.*, **92** (2020), 214–217. https://doi.org/10.1016/j.ijid.2020.01.050

4. S. Zhao, S. S. Musa, Q. Lin, J. Ran, G. Yang, W. Wang, et al., Estimating the unreported number of novel coronavirus (2019-nCoV) cases in China in the first half of January 2020: A data-driven modelling analysis of the early outbreak, *J. Clin. Med.*, **9** (2020), 388. https://doi.org/10.3390/jcm9020388

5. A. Parasher, COVID-19: Current understanding of its pathophysiology, clinical presentation and treatment, *Postgrad. Med. J.*, **97** (2021), 312–320. https://doi.org10.1136/postgradmedj-2020-138577

6. W. M. El-Sadr, A. Vasan, A. El-Mohandes, Facing the new Covid-19 reality, *N. Engl. J. Med.*, **388** (2023), 385–387. https://doi.org/10.1056/NEJMp2213920

7. I. Nesteruk, Statistics based predictions of coronavirus 2019-nCoV spreading in mainland China, 2020. MedRxiv.

8. K. Shah, R. U. Din, W. Deebani, P. Kumam, Z. Shah, On nonlinear classical and fractional order dynamical system addressing COVID-19, *Results Phys.*, **24** (2021), 104069. https://doi.org/10.1016/j.rinp.2021.104069

9. A. J. Lotka, Contribution to the theory of periodic reactions, *J. Phys. Chem.*, **14** (2002), 271–274. https://doi.org/10.1021/j150111a004

10. N. S. Goel, S. C. Maitra, E. W. Montroll, On the Volterra and other nonlinear models of interacting populations, *Rev. Mod. phys.*, **43** (1971), 231–276. https://doi.org/10.1103/RevModPhys.43.231

11. M. M. Khalsaraei, An improvement on the positivity results for 2-stage explicit Runge-Kutta methods, *J. Comput. Appl. Math.*, **235** (2010), 137–143. https://doi.org/10.1016/j.cam.2010.05.020

12. P. Zhou, X. L. Yang, X. G. Wang, B. Hu, L. Zhang, W. Zhang, et al., A pneumonia outbreak associated with a new coronavirus of probable bat origin, *Nature*, **579** (2020), 270–273. https://doi.org/10.1038/s41586-020-2012-7

13. Q. Li, X. Guan, P. Wu, X. Wang, L. Zhou, Y. Tong, et al., Early transmission dynamics in Wuhan, China, of novel coronavirus infected pneumonia, *N. Engl. J. Med.*, **382** (2020), 1199–1207. https://doi.org/10.1056/NEJMoa2001316

14. I. I. Bogoch, A. Watts, A. Thomas-Bachli, C. Huber, M. U. G. Kraemer, K. Khan, Pneumonia of unknown aetiology in Wuhan, China: Potential for international spread via commercial air travel, *J. Travel Med.*, **27** (2020), taaa008. https://doi.org/10.1093/jtm/taaa008

15. A. B. Gumel, S. Ruan, T. Day, J. Watmough, F. Brauer, P van den Driessche, et al., Modelling strategies for controlling SARS out breaks, *Proc. Biol. Sci.*, **271** (2004), 2223–2232. https://doi.org/10.1098/rspb.2004.2800

16. R. Kahn, I. Holmdahl, S. Reddy, J. Jernigan, M. J. Mina, R. B. Slayton, Mathematical modeling to inform vaccination strategies and testing approaches for coronavirus disease 2019 (COVID-19) in nursing homes, *Clin. Infect. Dis.*, **74** (2022), 597–603. https://doi.org/10.1093/cid/ciab517

17. J. Mondal, S. Khajanchi, Mathematical modeling and optimal intervention strategies of the COVID-19 outbreak, *Nonlinear Dyn.*, **2022** (2022), 177–202. https://doi.org/10.1007/s11071-022-07235-7

18. A. I. Abioye, O. J. Peter, H. A. Ogunseye, F. A. Oguntolu, T. A. Ayoola, A. O. Oladapo, A fractional-order mathematical model for malaria and COVID-19 co-infection dynamics. *Healthc. Anal.*, **4** (2023), 100210. https://doi.org/10.1016/j.health.2023.100210

19. J. T. Wu, K. Leung, G. M. Leung, Nowcasting and forecasting the potential domestic and international spread of the 2019-nCoV outbreak originating in Wuhan, China: A modelling study, *Lancet*, **395** (2020), 689–697. https://doi.org/10.1016/S0140-6736(20)30260-9

20. J. T. Machado, V. Kiryakova, F. Mainardi, Recent history of fractional calculus, *Commun. Nonlinear Sci. Numer. Simul.*, **16** (2011), 1140–1153. https://doi.org/10.1016/j.cnsns.2010.05.027

21. F. C. Meral, T. J. Royston, R. Magin, Fractional calculus in viscoelasticity: An experimental study, *Commun. Nonlinear Sci. Numer. Simul.*, **15** (2010), 939–945. https://doi.org/10.1016/j.cnsns.2009.05.004

22. R. L. Magin, Fractional calculus in bioengineering, *Crit. Rev. Biomed. Eng.*, **32** (2004), 1–104. https://doi.org/10.1615/critrevbiomedeng.v32.i1.10

23. M. Dalir, M. Bashour, Applications of fractional calculus, *Appl. Math. Sci.*, **4** (2010), 1021–1032.

24. R. L. Magin, *Fractional calculus in bioengineering*, Redding: Begell House, 2006.

25. Y. A. Rossikhin, M. V. Shitikova, Applications of fractional calculus to dynamic problems of linear and nonlinear hereditary mechanics of solids, *Appl. Mech. Rev.*, **50** (1997), 15–67. https://doi.org/10.1115/1.3101682

26. R. Gorenflo, F. Mainardi, Fractional calculus. In: *Fractals and fractional calculus in continuum mechanics*, Vienna: Springer, 1997. https://doi.org/10.1007/978-3-7091-2664-6

27. E. Addai, A. Adeniji, O. J. Peter, J. O Agbaje, K. Oshinubi, Dynamics of age-structure smoking models with government intervention coverage under fractal-fractional order derivatives, *Fractal Fract.*, **7** (2023), 370. https://doi.org/10.3390/fractalfract7050370

28. M. Shimizu, W. Zhang, Fractional calculus approach to dynamic problems of viscoelastic materials. *JSME Int. J. Ser. C Mech. Syst. Mach. Elem. Manuf.*, **42** (1999), 825–837. https://doi.org/10.1299/jsmec.42.825

29. F. Mainardi, An historical perspective on fractional calculus in linear viscoelasticity, *Fract. Calc. Appl. Anal.*, **15** (2012), 712–717. https://doi.org/10.2478/s13540-012-0048-6

30. Z. Dai, Y. Peng, H. A. Mansy, R. H. Sandler, T. J Royston, A model of lung parenchyma stress relaxation using fractional viscoelasticity, *Med. Eng. Phys.*, **37** (2015), 752–758. https://doi.org/10.1016/j.medengphy.2015.05.003

31. M. M. Amirian, Y. Jamali, The concepts and applications of fractional order differential calculus in modeling of viscoelastic systems: A primer, *Crit. Rev. Biomed. Eng.*, **47** (2019), 249–276. https://doi.org/10.1615/CritRevBiomedEng.2018028368

32. H. Khan, J. F. Gómez-Aguilar, A. Alkhazzan, A. Khan, A fractional order HIV-TB coinfection model with nonsingular Mittag-Leffler law, *Math. Method. Appl. Sci.*, **43** (2020), 3786–3806. https://doi.org/10.1002/mma.6155

33. C. Celauro, C. Fecarotti, A. Pirrotta, A. C. Collop, Experimental validation of a fractional model for creep/recovery testing of asphalt mixtures, *Constr. Build. Mater.*, **36** (2012), 458–466. https://doi.org/10.1016/j.conbuildmat.2012.04.028

34. G. C. Wu, M. Luo, L. L. Huang, S. Banerjee, Short memory fractional differential equations for new memristor and neural network design, *Nonlinear Dyn.*, **100** (2020), 3611–3623. https://doi.org/10.1007/s11071-020-05572-z

35. A. Atangana, D. Baleanu, New fractional derivatives with non-local and non-singular kernel, 2016. arXiv:1602.03408.

36. E. F. D. Goufo, Application of the Caputo-Fabrizio fractional derivative without singular kernel to Korteweg-de Vries-Burgers equation, *Math. Model. Anal.*, **21** (2016), 188–198. https://doi.org/10.3846/13926292.2016.1145607

37. E. F. D. Goufo, A biomathematical view on the fractional dynamics of cellulose degradation, *Fract. Calc. Appl. Anal.*, **18** (2015), 554–564. https://doi.org/10.1515/fca-2015-0034

38. M. B. Jeelani, Stability and computational analysis of COVID-19 using a higher order galerkin time discretization scheme, *Adv. Appl. Stat.*, **86** (2023), 167–206. https://doi.org/10.17654/0972361723022

39. A. Al Elaiw, F. Hafeez, M. B. Jeelani, M. Awadalla, K. Abuasbeh, Existence and uniqueness results for mixed derivative involving fractional operators, *AIMS Mathematics*, **8** (2023), 7377–7393. https://doi.org/10.3934/math.2023371

40. S. K. Kabunga, E. F. D. Goufo, V. H. Tuong. Analysis and simulation of a mathematical model of tuberculosis transmission in democratic Republic of the Congo, *Adv. Differ. Equ.*, **2020** (2020), 642. https://doi.org/10.1186/s13662-020-03091-0

41. A. Atangana, S. I. Araz, Mathematical model of COVID-19 spread in Turkey and South Africa: Theory, methods and applications, *Adv. Differ. Equ.*, **2020** (2020), 659. https://doi.org/10.1186/s13662-020-03095-w

42. A. Atangana, S. I. Araz, New concept in calculus: Piecewise differential and integral operators, *Chaos Soliton. Fract.*, **145** (2021), 110638. https://doi.org/10.1016/j.chaos.2020.110638

43. M. A. Khan, A. Atangana, Modeling the dynamics of novel coronavirus (2019-nCov) with fractional derivative, *Alex. Eng. J.*, **59** (2020), 2379–2389. https://doi.org/10.1016/j.aej.2020.02.033

44. M. A. Khan, A. Atangana, E. Alzahrani, Fatmawati, The dynamics of COVID-19 with quarantined and isolation, *Adv. Differ. Equ.*, **2020** (2020), 425. https://doi.org/10.1186/s13662-020-02882-9

45. O. Dyer, Covid-19: China stops counting cases as models predict a million or more deaths, *BMJ*, **380** (2023), 2. https://doi.org/10.1136/bmj.p2

46. A. Moumen, R. Shafqat, A. Alsinai, H. Boulares, M. Cancan, M. B. Jeelani, Analysis of fractional stochastic evolution equations by using Hilfer derivative of finite approximate controllability, *AIMS Mathematics*, **8** (2023), 16094–16114. https://doi.org/10.3934/math.2023821

47. A. Zeb, A. Atangana, Z. A. Khan, S. Djillali, A robust study of a piecewise fractional order COVID-19 mathematical model, *Alex. Eng. J.*, **61** (2022), 5649–5665. https://doi.org/10.1016/j.aej.2021.11.039

48. C. Y. Li, J. Yin, A pedestrian-based model for simulating COVID-19 transmission on college campus, *Transportmetrica A*, **19** (2023), 2005182. https://doi.org/10.1080/23249935.2021.2005182

49. M. S. Arshad, D. Baleanu, M. B. Riaz, M. Abbas, A novel 2-stage fractional Runge-Kutta method for a time fractional logistic growth model, *Discrete Dyn. Nat. Soc.*, **2020** (2020), 1020472. https://doi.org/10.1155/2020/1020472
50. F. Liu, K. Burrage, Novel techniques in parameter estimation for fractional dynamical models arising from biological systems, *Comput. Math. Appl.*, **62** (2011), 822–833. https://doi.org/10.1016/j.camwa.2011.03.002
51. M. T. Hoang, O. F. Egbelowo, Dynamics of a fractional-order hepatitis B epidemic model and its solutions by nonstandard numerical schemes, In: *Mathematical Modelling and Analysis of Infectious Diseases*, Springer, Cham, **302** (2020), 127–153. https://doi.org/10.1007/978-3-030-49896-2_5
52. Z. J. Fu, Z. C. Tang, H. T. Zhao, P. W. Li, T. Rabczuk, Numerical solutions of the coupled unsteady nonlinear convection-diffusion equations based on generalized finite difference method, *Eur. Phys. J. Plus*, **134** (2019), 272. https://doi.org/10.1140/epjp/i2019-12786-7
53. B. Wang, L. Li, Y. Wang, An efficient nonstandard finite difference scheme for chaotic fractional-order Chen system, *IEEE Access*, **8** (2020), 98410–98421. https://doi.org/10.1109/ACCESS.2020.2996271
54. A. J. Arenas, G. González-Parra, B. M. Chen-Charpentier, Construction of nonstandard finite difference schemes for the SI and SIR epidemic models of fractional order, *Math. Comput. Simulat.*, **121** (2016), 48–63. https://doi.org/10.1016/j.matcom.2015.09.001
55. R. Lewandowski, Z. Pawlak, Dynamic analysis of frames with viscoelastic dampers modelled by rheological models with fractional derivatives, *J. Sound Vib.*, **330** (2011), 923–936. https://doi.org/10.1016/j.jsv.2010.09.017
56. Pakistan population (LIVE), Available from: `https://www.worldometers.info/world-population/pakistan-population/`.
57. Pakistan COVID-19 corona tracker, Available from: `https://www.coronatracker.com/country/pakistan/`.
58. Current information about COVID-19 in Pakistan, Available from: `https://www.worldometers.info/`.
59. K. Shah, T. Abdeljawad, R. Ud Din, To study the transmission dynamic of SARS-CoV-2 using nonlinear saturated incidence rate, *Physica A*, **604** (2022), 127915. https://doi.org/10.1016/j.physa.2022.127915
60. R. Ouncharoen, K. Shah, R. Ud Din, T. Abdeljawad, A. Ahmadian, S. Salahshour, et al., Study of integer and fractional order COVID-19 mathematical model, *Fractals*, **31** (2023), 2340046. https://doi.org/10.1142/S0218348X23400467

AIMS Press